

NICMOS Two Gyro Mode Coronagraphic Performance

G. Schneider, A.B. Schultz, S. Malhotra, I. Dashevsky
July 8, 2005

ABSTRACT

In preparation for the Hubble Space Telescope (HST) entry into Two Gyro Mode (TGM) operations, the NICMOS coronagraphic performance was assessed during the February 21, 2005 TGM on orbit test (ID: 10448) in two filter bands (F110W and F160W). The gyroscope pair 2-4 was used for the TGM test. Observations were obtained of a previously observed calibration target (GJ517; sp.type=K5Ve) coronagraphically and with direct imaging. The F110W filter performance very closely tracks the three gyro mode (ID: 10177) results. The observed jitter of ~ 6.2 mas had little effect on the $1.1 \mu\text{m}$ coronagraphy. This result clearly shows that $1.1 \mu\text{m}$ coronagraphy is robust against the observed TGM jitter. The NICMOS coronagraph inner working angle (IWA) is $3.2 \lambda/D$ at $1.1 \mu\text{m}$. Consequently, there is sufficient performance compliance to target decentering of these RMS amplitudes within the coronagraphic hole. There was a slight decline in performance with the F160W filter with respect to three gyro mode which may be due to imaging systematics; i.e., breathing and jitter. The $1.6 \mu\text{m}$ coronagraphy is more susceptible to imaging systematics primarily due its broader PSF (IWA= $2.2 \lambda/D$). At $r=10$ pixels, the coronagraphic diffracted and scattered light suppression factor is ~ 3 compared to direct imaging, while it is a factor of 4 in three gyro mode. The observed coronagraphic performance is essentially unaffected at $1.1 \mu\text{m}$ with TGM operations, while there is a marginal decline at $1.6 \mu\text{m}$ of similar amplitude to that arising from other well-known HST/NICMOS orbit-driven instabilities. The improvement in image contrast (and dynamic range) with coronagraphy and TGM is still substantial over direct imaging.

Introduction

The performance of the Near Infrared Camera and Multi-Object Spectrometer (NICMOS) Camera 2 coronagraphic observing mode is sensitive to small target centering errors within the coronagraphic hole. The NICMOS coronagraph employs a 165 μm diameter hole in the Camera 2 Field Divider Mirror (outside the dewar) at the HST F/24 focus. Coronagraphic targets are blind pointed into an acquisition subarray in the NIC2 camera away from the hole. The NICMOS Mode-2 target acquisition process locates the position of the target and the hole on the detector. A target-hole position offset is determined and the telescope is slewed to move the image of the target into the hole (Schultz et al. 1998, Schneider 2002). The coronagraphic imaging mode was fully reactivated following Hubble Space Telescope (HST) Servicing Mission 3B (SM3B) and its performance was comparable to HST Cycle 7 but with improved Quantum Efficiency (Schultz et al. 2004).

The flight software's (FSW's) photocentric determination of the position of the hole is not the point at which an occulted target will have its total diffracted+scattered energy minimized by established criteria. The "low scatter point" (referred to as the "sweet spot") is offset from the hole photocenter by a small amount ($x=-0.75$, $y=-0.05$ pixels). The hole image on the detector is 0.3" in radius (~ 4 pixels). The calibration test program (ID: 9693) results indicated that the test target was robustly acquired within approximately 0.08 pixel (~ 5.8 mas) of the absolute low-scatter position, with a repeatability of 0.04 pixel (~ 2.9 mas), which meets the requirement given the error budget for onboard processing of target acquisition images.

FGS Guiding

There are three Fine Guidance Sensors (FGS) onboard HST. They provide high precision pointing control by using guide stars to actively control the telescope pointing. Two guide stars are required to maintain telescope pointing (attitude) and roll (orientation) control at a level of precision required for NICMOS coronagraphy. At the start of the coronagraphic visit, the FGSs find and acquire the guide stars to establish HST pointing control. The NICMOS onboard target acquisition removes absolute uncertainties in the target placement due to Guide Star Catalogue (GSC) position uncertainties. With two FGSs and three gyroscopes providing input to the vehicle pointing control law the optical line-of-sight is maintained with a stability of a few milli-arc seconds (mas).

On rare occurrences, an orbital disturbance (e.g. a micro-meteor hit) can change the pointing of the telescope. The FGSs will track the movement of the guide stars in their FOVs and return the telescope to the previous pointing. However, during a larger pointing disturbance, called a recentering event, the FGSs are commanded to release the guide stars. After the event, the FGSs are commanded to the last known position of the guide stars and guiding is resumed. This can cause a displacement in an FGS interferometric fringe visibility function, and result in a translation of the target on the detector.

Gyro Control

HST pointing control system (PCS) was designed to use three operational gyroscopes to position and maintain a science target within a Science Instrument's (SI) aperture with sufficient accuracy to obtain meaningful science data. HST currently has four of its six gyroscopes operational. Gyro 5 failed on April 28, 2001, and Gyro 3 failed on April 29, 2003.

Two gyros provide rate information only about two vehicle axes. Therefore, another sensor is required to estimate the rates about the third axis. The options available are the Coarse Sun Sensors (CSSs), the Magnetic Sensing System (MSS), the Fixed Head Star Trackers (FHST), and the Fine Guidance Sensors (FGSs). Following a review of the different Pointing Control System (PCS) options, the FGS was selected as the instrument to provide the rate information for the axis normal to the plane defined by the two operational gyros. FGS data in either Coarse Track (CT) or Fine Lock (FL) readout modes can be used by the control law. After FGS acquisition of a star and valid star position data are available, FGS measurements are input into the HST attitude control law. These measurement will essentially replace the missing gyroscope data.

The FGS telemetry and the gyro data at 40 Hz are input into the attitude control law. In this mode, the 1- σ pointing stability was expected to be ~ 30 mas (Anandakrishnan et al. 2003). The actual on-orbit TGM average jitter (60 sec RMS) for the 2-4 gyro pair was ~ 6.2 mas with a maximum jitter of ~ 7.3 mas. Using a 10 sec average instead of a 60 sec average, the jitter was ~ 6.1 - 8.8 mas. The jitter during the TGM test was comparable to three gyro mode jitter (Clapp 2005).

Data

The calibration target GJ 517 (Sp=K5Ve) was observed coronagraphically under three gyro mode (ID: 10177 visit 82) and two gyro mode (ID: 10448) control. Target characteristics are presented in Table 1. Under three gyro mode control, GJ517 was observed coronagraphically and directly within a single orbit. Under two gyro mode control, it was acquired coronagraphically twice within an orbit, at the start and end of the visibility period. And GJ 517 was also displaced from the hole and observed directly to access the stability of the position and accuracy of the target in the hole. Observations were repeated in back-to-back orbits with a roll (29.9°) between orbits. Observations were obtained in the F110W and F160W filters. The F110W filter provides the best spatial resolution ($\sim 0.12''$ FWHM) and is of particular use for circumstellar disk imaging. This filter also minimizes the spatial extent of the background residuals from the PSF. The F160W filter is particularly useful for detection and imaging of substellar (L and T dwarfs and extrasolar giant planets) companions to M dwarfs, and to young substellar companions for earlier spectral type stars.

The data were fast tracked to a holding disk to expedite the reduction and analysis. Two teams, one at STScI and another at Steward Observatory, University of Arizona, Tucson, AZ, calibrated, reduced, and analyzed the data.

Table 1. GJ517 target characteristics.

target name	spc. type	V	J	H	K
GJ 517	K5Ve	9.31	6.88	6.31	6.12

Cycle 7 GTO/7226 Data - Calibration Target Pedgree

Observations of GJ 517 in GTO program 7226 were obtained using the “two-orientation per visibility period” observing mode. The F171M filter target acquisition images confirmed the singular nature of the target (to the detectability limits of HST/NICMOS at $1.7 \mu\text{m}$, $\sim 0.08''$ for near-equal magnitude components; which is half a resolution element). No point-like objects were seen in the vicinity of the star to the 2-roll F160W filter coronagraphic detection limits (Schneider and Silverstone 2003). Later, inter-target flux-scaled PSF subtractions found no detectable circumstellar disk excess due to dust (scattering fractions $> \sim 10^{-5}$ detectable).

GJ 517 was the 6th coronagraphic science target to be observed with NICMOS, observed on 23 March 1998. At the time of the GJ 517 observations an infamous NICMOS FSW “decentering” bug had not yet been eradicated. Fortunately, differential miscenterings resulting from this later fixed FSW problem were relatively small for GJ 517 and did not adversely affect the coronagraphic performance. The targeting performance for those observations (along with all of the other affected observations) were reported to STScI and GSFC Code 512 in 1998 by the NICMOS IDT as part of the analysis of the FSW problem. For these reasons, acquisition and coronagraphic performance in the TGM test should be compared to the most recent Cycle 13 observations.

Cycle 13 GO/10177 Data

GJ 517 is one of four coronagraphic PSF calibrators in GO proposal 10177 for the reasons stated above (and the need for a bright calibration target of mid-K spectral type for the science goals of the program). Deep (high S/N) coronagraphic as well as direct (“out of hole”, but PSF core saturated) images of GJ 517 were obtained as part of the proposal 10177 calibration plan in the F110W and F160W filters on 20 January 2005 (Visit 82). Reference data were provided for the TGM performance test by the GO/10177 team. These coronagraphic PSF calibration observations were executed after the recent OTA secondary mirror adjustment on 22 December 2004, and hence are appropriate to use as baseline observations for assessing coronagraphic performance under two-gyro guiding.

Data were calibrated, reduced, and processed by the team members for proposal 10177. The Interactive Data Language (IDL) package of routines called **IDP3** (Schneider and Stobie 2002) was used for registering and manipulating images. Table 2 presents a list of the 10177 data.

Table 2. 10177 visit 82 GJ 517 coronagraphic and direct imaging observations.

Obs	Filter	Exptime (sec)	Num Exp	Comments
n8zu82q7q	F171M	0.29	1	ACQ
n8zu82q8q	F160W	31.95	1	
n8zu82q9q-dq	F160W	223.96	5	
n8zu82qfq	F110W	31.95	1	
n8zu82qgq-kq	F110W	223.96	5	
n8zu82qmq-nq	F110W	2.03	2	POS TARG 2, 2
n8zu82qoq-pq	F110W	2.03	2	POS TARG 2,-2
n8zu82qqq-rq	F160W	2.03	2	POS TARG 2,-2
n8zu82qsq-tq	F160W	2.03	2	POS TARG -2, 2

Direct and coronagraphic calibrated images of GJ 517 are presented in Figure 1. For each filter, the direct and coronagraphic images shown were intensity-normalized to the azimuthally medianed per pixel intensity at $r = 4.0$ pixels from the center of the non-coronagraphic direct PSF image. The normalization factors were $1/5499.1$ and $1/9146.3$ ADU sec^{-1} pixel^{-1} , for F110W and F160W filter images, respectively.

Radial Profiles for the F110W and F160W filter, direct to coronagraphic comparisons, are presented in Figure 2. Individual profiles were computed as azimuthally median count rates per-pixel in incrementing radial zones about the target positions. The images were 8x sub-pixel resampled (via sinc-function apodized bi-cubic interpolation) to provide higher granularity in the radial profiling (and verified with comparison to unresampled profiles). These data were NOT geometrically rectified to compensate for the approximate 0.7% difference in the X and Y pixel scales, and as such profiling in detail, is in incremental units of pixels - not sky-projected arc-seconds (noting the difference is very small, and not significant for the metrical comparisons presented here).

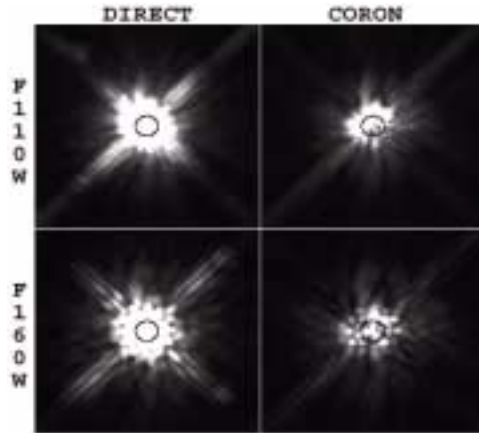


Figure 1: GJ 517 (ID: 10177, visit 82) direct and coronagraphic images, 80 x 80 pixels (~6" x 6") regions centered on the target locations. Top row F110W filter images and bottom row F160W filter images. "Hard white" corresponds to display not data saturation. Black circle is 0.3" in radius corresponding to the size of the coronagraphic hole.

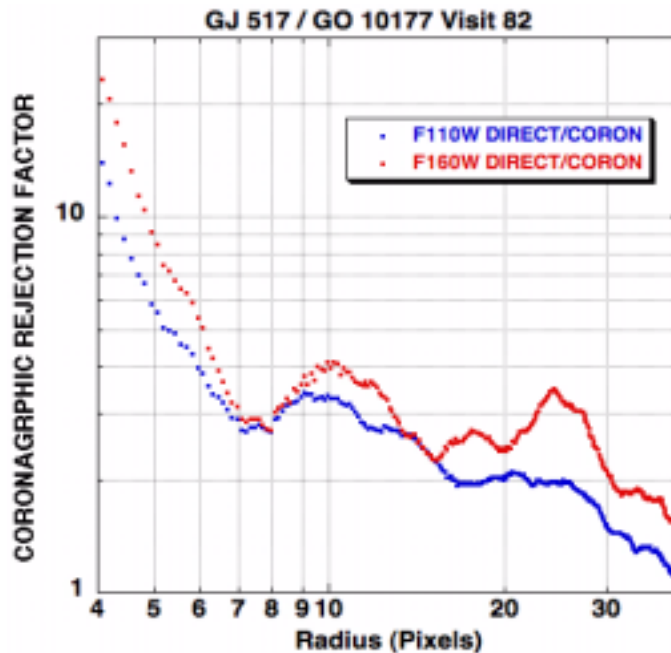


Figure 2: GJ 517 (ID: 10177, visit 82) direct to coronagraphic radial profile comparisons. Upper curve F160W (1.6 μm), lower curve F110W (1.1 μm). Individual profiles computed as azimuthally median count rates per-pixel in incrementing radial zones about the target positions. Four pixels is at the approximate edge of the coronagraphic hole (radius=0.3").

Coronagraphic Performance

Figure 2 shows the coronagraphic performance (scattered and diffracted light rejection by the coronagraph) at 1.1 μm (F110W) and 1.6 μm (F160W) using three gyro mode guid-

ing. At 1.1 μm , the coronagraphic performance ranges from ~ 3 times better than direct imaging at 8-10 pixels to a gradual fall off to ~ 2 times better at larger distances from the coronagraphic hole. At 1.6 μm , the coronagraphic performance is more dependent upon imaging systematics; i.e., breathing, cold mask instabilities and other effects on orbit and at longer timescales. Coronagraphic performance ranges from ~ 4 times better than direct imaging at 9-12 pixels, drops slightly to ~ 2 times better at ~ 18 pixels, and then rises to ~ 3.5 times better at ~ 25 pixels from the hole. One should not over interpret the 1.6 μm performance due to the imaging systematics at the time of the observations. The drop off at large distances from the hole is primarily due to the lack of photons.

Two Gyro Mode Coronagraphic Performance Test

The Two Gyro Mode (TGM) test executed successfully on 21-23 February 2005. After completion of the TGM test, the nominal three gyro control law was restored. HST science resumed on Thursday 24 February 2005. The NICMOS TGM coronagraphic test program 10448 executed on 21 February 2005. Direct and coronagraphic observations of GJ 517 were obtained. FGS guide star acquisitions were successful and no guiding anomalies were reported. Table 3 and 4 presents a list of the data.

UA Data Reduction

For each filter, the coronagraphic images were median combined within each visit. The coronagraphic target position in SIAF pixel coordinates was determined from the ACQ images and the Mode-2 targeting slew. The direct images (PSF-core saturated images at the coronagraphic focus) were median combined after registration. Registration was accomplished in the same manner as the 20 January 2005 images (ID: 10177 visit 82) using the post-coronagraphic "world coordinate" pointing offset information associated with the direct image data files. The pixel coordinates of the core-saturated target were determined from the preplanned small angle maneuvers (SAMs) (via the POS TARG and Patterns). The offsets were verified (measured) both absolutely and differentially with the one unocculted stellar image visible in both the direct and coronagraphic frames at the very edge of the field in Visit 01. Because of the four-point dither combinations, the size of the direct image mosaics were larger than the undithered frames. The data were calibrated, reduced, and processed by G. Schneider (UA). The Interactive Data Language (IDL) package of routines called **IDP3** was used for registering and manipulating images. Details of the UA image processing and analysis maybe be found at: http://nicmosis.as.arizona.edu:8000/2GYRO_CALIBRATION/2GYRO.html#10448

STScI Data Reduction

No additional calibration steps were performed to the data. The OPUS pipeline calibration uses the most up-to-date calibration files and processing routines. Software tools from the STSDAS mstools package were used for data reduction; i.e., **msarith**, **mscom-**

bine, and **mssplit**. The coronagraphic target position was determined using the Mode-2 ACQ target position and slew maneuver. This information is stored in the science headers. The position of the target in the direct images was determined from the BLANK filter (dark) observations which contain persistence images of the target at each position of the pattern. The IRAF task **imcentroid** was used for centroiding and the task **imshift** was used for image registration.

Table 3. 10448 visit 01 GJ 517 coronagraphic and direct imaging observations.

Obs	Filter	Exptime (sec)	Num Exp	Comments
n99501epq	F171M	0.29	1	ACQ
n99501eqq	F110W	223.96	1	
n99501erq	F160W	223.96	1	
n99501esq	F110W	223.96	1	
n99501etq	F160W	223.96	1	
n99501euq	F110W	223.96	1	
n99501evq	F160W	223.96	1	
n99501eyq-f1q	F110W	2.03	1	POS TARG 4,-5 PATTERN 01
n99501f2q-4q	BLANK	14.27	2	POS TARG 4,-5
n99501f5q-8q	F160W	2.03	1	POS TARG 4.5,-5.5 PATTERN 02
n99501f9q	F171M	0.29	1	ACQ

Table 4. 10448 visit 02 GJ 517 coronagraphic and direct imaging observations.

Obs	Filter	Exptime (sec)	Num Exp	Comments
n99502fbq	F171M	0.29	1	ACQ
n99502fcq	F110W	223.96	1	
n99502fdq	F160W	223.96	1	
n99502feq	F110W	223.96	1	
n99502ffq	F160W	223.96	1	
n99502fgq	F110W	223.96	1	
n99502fhq	F160W	223.96	1	

Obs	Filter	Exptime (sec)	Num Exp	Comments
n99502fjq-mq	F110W	2.03	1	POS TARG 4,-5 PATTERN 01
n99502fnq-pq	BLANK	14.27	2	POS TARG 4.5,-5.5
n99502fqq-tq	F160W	2.03	1	POS TARG 4.5,-5.5 PATTERN 02
n99502fuq	F171M	0.29	1	ACQ

TGM Coronagraphic Performance

Figure 3 presents the coronagraphic performance using two gyro guiding; i.e., the ratio of individual azimuthally averaged PSF radial intensity profiles between direct and coronagraphic imaging. The TGM curves for both filters (F110W, F160W) repeat extremely well between orbits which shows the stability and repeatability of the pointing and the imaging systematics.

The TGM 1.1 μm coronagraphic performance tracks the 1.1 μm three gyro coronagraphic performance. This indicates that the 1.1 μm coronagraphy is robust against RMS jitter of ~ 6.2 mas. The TGM jitter had little effect on the 1.1 μm coronagraphy. The coronagraph is $3.2 \lambda/D$ at 1.1 μm , hence compliant. Compliance to decentering at this level is true not only for diffractive suppression, but "hole edge scattering" as the first Airy ring is well contained in the image-plane hole even with jitter of these levels.

The TGM 1.6 μm coronagraphic performance indicates a slight decline in performance in two gyro mode with respect to three gyro mode. As mentioned above, at 1.6 μm , the coronagraphic performance is more susceptible to imaging systematics; i.e., breathing, cold mask instabilities and other effects on orbit and at longer domestically. At $r=10$ pixels, the coronagraphic suppression factor is 3 compared to direct imaging, and is a factor of 4 in three gyro mode. At $r=20$ pixels, the coronagraphic suppression factor is 2 compared to direct imaging, and is a factor of 2.4 in three gyro mode. The magnitude of the reduction in coronagraphic rejection still results in significant gains in image contrast over direct imaging.

Breathing & Cold Mask Movement

Differences between the two gyroscope mode (21 February 2005) and three gyroscope mode (20 January 2005) direct to coronagraphic radial profile comparisons of 1/3 or less can be attributed to differential breathing and cold mask motions at the $1-\sigma$ level, but cannot be "decoupled" from two versus three gyro mode performance. With this caveat regarding the statistical significance of the measures with respect to the unresolved systematics, the 1.6 μm data in two gyro mode are, in general, not significantly different than

those in three gyro mode. This is completely consistent with the expectation that the RMS jitter during the coronagraphic integration would be $< \sim 7\text{-}8$ mas.

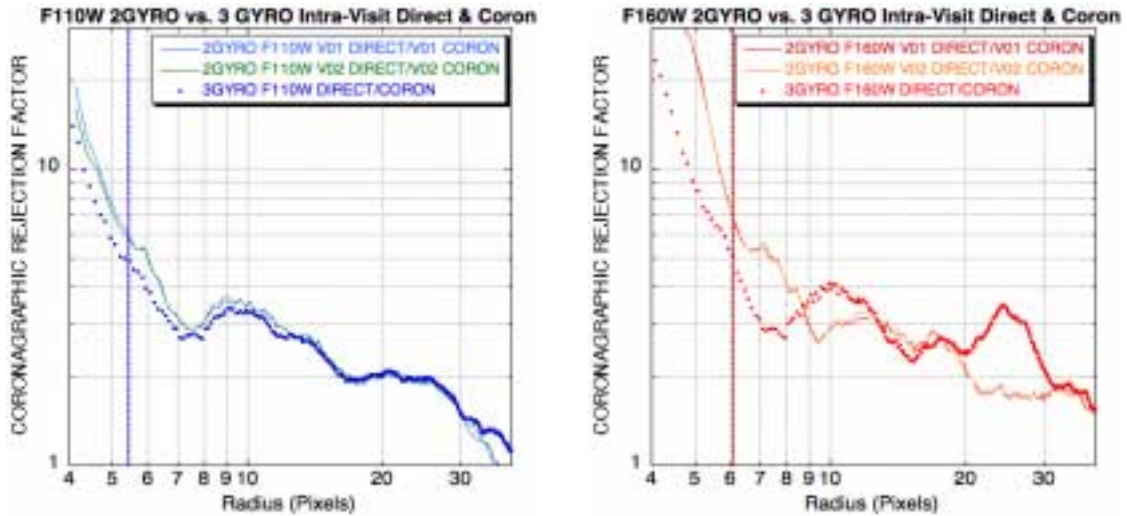


Figure 3: GJ 517 (ID: 10448) direct to coronagraphic radial profile comparisons. Left F110W (1.1 μm) and right F160W (1.6 μm) coronagraphic performance. Individual profiles computed as azimuthally median count rates per-pixel in incrementing radial zones about the target positions. Four pixels is at the approximate edge of the coronagraphic hole (radius=0.3"). The dotted vertical lines represent a full resolution element (1.45 and 2.11 pixels) away from the edge of the hole for F110W and F160W, respectively.

Conclusions

The two gyroscope mode (TGM) coronagraphic performance test (ID: 10448) obtained direct and coronagraphic observations of a previously observed calibration target (GJ517; sp.type=K5Ve). The gyroscope pair 2-4 was used for the test. The results of the TGM test **clearly shows** that coronagraphic performance is essentially unaffected at 1.1 μm (F110W), while there is a marginal decline at $8 < r < 12$ pixels and at $18 < r < 32$ pixels at 1.6 μm (F160W). The statistical significance of the 1.6 μm data with respect to the unresolved systematics in two gyro mode are in general not significantly different than those in three gyro mode. This is completely consistent with the expectation that the RMS jitter during the coronagraphic integration would be $< \sim 7\text{-}8$ mas. However, within some limited radial zones (distances from the hole), the coronagraphic PSF subtraction actually has larger residuals than the direct imaging subtraction. This behavior has often been seen with coronagraphic PSF "mismatches" driven by OTA focus changes (breathing). The TGM results are still better than direct imaging subtraction.

Intra-orbit roll maneuvers are untenable with two gyro mode guiding. Thus, rolling the telescope within a single visibility period for coronagraphic PSF subtraction will not be allowed. Hence, the TGM program 10448 data provided a measure of the sequential-orbit

PSF subtraction with two gyro mode guiding. The TGM coronagraphic performance curves for both filters (F110W, F1160W) repeat extremely well between orbits which shows the stability and repeatability of the pointing and the imaging systematics. However, the results must be viewed very cautiously, as any effects from the two gyro mode guiding mode in these singular differential observations cannot be decoupled from other systematics which affect the temporal stability of the PSF on multi-orbit time scales.

Recommendations

The TGM test provided the information needed to access the coronagraphic performance and to allow observers to construct effective programs to maximize the signal-to-noise and minimize background residuals from coronagraphic observations. NICMOS Camera 2 coronagraphy with two gyro mode guiding will provide higher image contrasts than direct imaging. Cycle 14 and later coronagraphic observers should plan on two orbits per target, obtaining coronagraphic observations in back-to-back orbits for PSF subtractions. And for targets with circumstellar material or disks, observing PSF targets close in time to the prime target observations, preferably in adjacent orbits.

Acknowledgements

We would like to thank the STScI Spacecraft Systems Branch (SCSB) for detailed information on Two Gyro Mode (TGM). And we would like to thank Merle Reinhart, George Chapman (SPB), and Beth Perriello (OPB) for laying the ground work and scheduling for a successful observing program. We also would like to thank OPUS for fast tracking the TGM coronagraphic data to a holding disk.

References

Anandakrishnan, S.M., Clapp, B., Kimmer, E., Smith, D., and Wirzburger, J. 2003, "Baseline PCS Architecture and Requirements for Two Gyro Science," Engineering Memorandum, 3 July 2003, Mission Operations, Systems Engineering, & Software (MOSES) Program.

Clapp, B. 2005, viewgraph presentation, "TGS Project Briefing," March 2, 2005, 69.

Schultz, A.B., Noll, K., Storrs, A., Bacinski, JI, Baggett, W., and Fraquelli, D. 1998, "NICMOS Camera 2 Coronagraphic ACQs," NICMOS Instrument Science Report, NICMOS-98-012.

Schultz, A.B., Schneider, G., Dashevsky, I. Fraquelli, D., Welty, A., and Roye, E. 2004, "NICMOS Coronagraphic Calibration," NICMOS Instrument Science Report, NICMOS-04-001.

Schneider, G., 2002, "Coronagraphy with NICMOS", in The 2002 HST Calibration Workshop, eds. S. Arribas, A. Koekemoer, and B. Whitmore, (Space Telescope Science Institute, Baltimore, Maryland), 249.

Schneider, G. and Silverstone, M. 2003, "Coronagraphy with HST/NICMOS: detectability is a sensitive issue", in High-Contrast Imaging for Exo-Planet Detection, eds. A. B. Schultz & R. G. Lyon, SPIE Proceedings Series, 4860, 1.

Schneider, G. and Stobie, B. 2002, "Pushing the Envelope: Unleashing the Potential of High Contrast Imaging with HST", in ADASS XI, eds. D. A. Bohlender, D. Durand & T. H. Handley, ASP Conference Series, 281, 382.

Appendix I - Radial Profiles

In this section, a comparison of radial profiles, azimuthally averaged residual flux between the diffraction spikes, for single and PSF subtracted images are presented. The diffraction spikes were masked off, 8-pixels inclusive, and set to a very large negative number. This resulted in an inner radius for the radial profiles of 8-pixels ($\sim 0.6''$).

Figure 4 presents the radial profiles for the F110W and F160W filter direct and coronagraphic observations. Three different profiles are presented for each filter; i.e. target outside of hole, in the hole, and coronagraphic-coronagraphic subtraction. The coronagraphic images were obtained in back-to-back orbits with a 29.9° roll of the telescope at the start of the second orbit. The orbit 2 coronagraphic images were registered to and subtracted from the orbit 1 images. The hole image moved on the detector by a small amount between orbits ($\Delta x = -0.011$, $\Delta y = -0.004$ pixels).

The $1.1 \mu\text{m}$ (F110W) and $1.6 \mu\text{m}$ (F160W) radial profiles with the target located outside and inside the hole, receptivity, track very close together with exposure times of 2.0 sec for the direct imaging and 224 sec for the target in the coronagraphic hole. For each filter, a gain of ~ 0.5 magnitude per pixel in light suppression is obtained for placement of the target in the coronagraphic hole.

The $1.1 \mu\text{m}$ (F110W) coronagraphic-coronagraphic subtraction profile indicates a good subtraction to an inner radial distance of ~ 8 pixels ($0.6''$), while the $1.6 \mu\text{m}$ (F160W) profile indicates a good subtraction to an inner radius of ~ 14 pixels ($1.0''$). Not surprisingly, the $1.6 \mu\text{m}$ (F160W) results are similar to those reported by Schultz et al (1999) for coronagraphic-coronagraphic subtraction of images obtained in back-to-back orbits with a roll of the telescope between orbits.

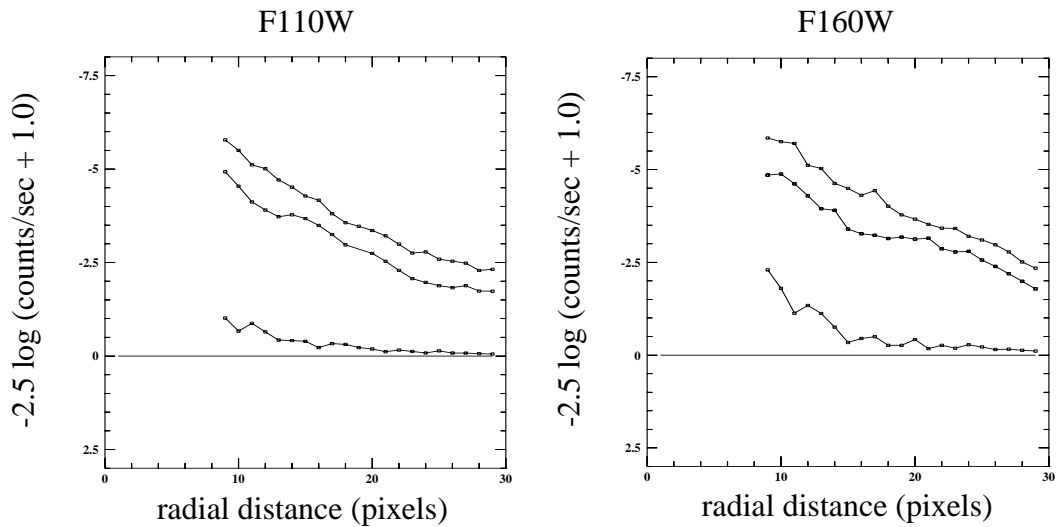


Figure 4: GJ 517 (ID: 10448) radial profiles (pixels) centered on target locations. Profiles are azimuthally averaged residual flux between the diffraction spikes. Top profile, direct image; middle profile, target in coronagraphic hole; and bottom profile, orbit 2 coronagraphic image registered and subtracted from orbit 1 image.

The GJ 517 (ID: 10448) orbit 1 and 2 observations were identical; i.e., respective filter observations were obtained in identical portions of the orbit. And they were obtained in identical time sequences following the NICMOS onboard ACQ. Each orbit required a different set of guide stars. There was no change in time sequence due to guide star acquisitions. Movement of the coronagraphic hole between orbits was minimal. Yet, orbit 2 images needed to be shifted to register them with the orbit 1 images. Residuals remained when images were subtracted from each other. The light distribution within the diffraction spikes changed from orbit-to-orbit, quite possibly due to small subpixel shifts of the PSF on the array. Most likely breathing, a change in the HST focus position, movement of the Camera 2 cold mask at the pupil (Lyot stop), and/or to other imaging systematics caused the light distribution differences in the PSF between orbits.

There is no a priori way to know in advance the change in attitude of the telescope, phase and amplitude of the OTA breathing and the Sun angle and roll changes, from the previous target to the coronagraphic target until the observations are scheduled on a calendar, a Science Mission Schedule (SMS). The attitude history preceding the coronagraphic observations has a large affect upon the success or failure for PSF subtraction. And it seems that time dependent changes will affect back-to-back orbit coronagraphic observations. See NICMOS Instrument Science Report (ISR) ISR-99-006, “NICMOS Coronagraphic Imaging Strategy” for additional information.

url:<http://www.stsci.edu/hst/nicmos/documents/isrs>